DALTON
FULL PAPER

Electrochemical and spectroscopic studies on the reduction of the *cis*-$(Et_2$-dcbpy$)_2RuX_2$ series of photovoltaic sensitizer precursor complexes (Et_2-dcbpy = diethyl 2,2′-bipyridine-4,4′-dicarboxylate, X = Cl^-, I^-, NCS^-, CN^-)

Georg Wolfbauer, Alan M. Bond * and Douglas R. MacFarlane *

Department of Chemistry, Monash University, Clayton 3168, Victoria, Australia.
E-mail: A.Bond@sci.monash.edu.au; D.MacFarlane@sci.monash.edu.au

Received 26th August 1999, Accepted 11th October 1999

The series of $(Et_2$-dcbpy$)_2RuX_2$ complexes, where Et_2-dcbpy is diethyl 2,2′-bipyridine-4,4′-dicarboxylate and X = Cl^-, I^-, NCS^-, CN^-, and its reduced forms have been investigated voltammetrically and spectroscopically in dimethylformamide at 22 °C and at −58 °C. Four chemically reversible reduction processes were observed with short time scale voltammetric conditions for $(Et_2$-dcbpy$)_2Ru(CN)_2$. An interesting linear relationship was found between the reversible potentials and temperature. A simple conceptual model is provided that relates this potential–temperature dependence to "electron hopping" of spatially isolated electrons. Additional evidence for this model was found in UV/VIS/NIR spectra of $[(Et_2$-dcbpy$)_2Ru(CN)_2]^-$, generated in spectroelectrochemical experiments. A weak band at 3500 cm^{-1} is also evidence of "ligand hopping". As predicted, this band was absent for $[(Et_2$-dcbpy$)_2$-$Ru(CN)_2]^{2-}$. The electronic spectra of other complexes are also discussed and bands tentatively assigned. The initial reduction products were not stable on longer time scales. Electrospray mass spectrometry was employed to identify decomposition products. In the case of $(Et_2$-dcbpy$)_2Ru(CN)_2$, the main reaction path was de-esterification, yielding the deprotonated acid. Additionally, reductively induced ligand elimination was the preferred decomposition pathway for the reduced complexes where X = Cl^- and I^-. The chemical reversibility of voltammetric reductions decreased in the order X = CN^- > NCS^- > Cl^- > I^-.

1. Introduction

One of the best series of sensitizers[1] for use in photoelectrochemical cells has the structure *cis*-$(H_2$-dcbpy$)_2RuX_2$ (H_2-dcbpy = 2,2′-bipyridine-4,4′-dicarboxylic acid, X = halides and pseudohalides). Ideally, the reversible potentials of all the photosensitizer redox reductions should be known. However, unfortunately, the reductive electrochemistry[2] of highly surface active $(H_2$-dcbpy$)_2Ru(NCS)_2$ is more complicated than the oxidation[3] and determination of the reversible reduction potentials *via* simple use of voltammetric techniques is not possible. Alternative methods of calculation of the reduction potentials are therefore still needed.

Esterification of the acid groups results in an increased stability of the compounds and a recent synthetic approach[4] utilized the esterified ligand and eventually its hydrolysis to isolate the required *cis*-$(H_2$-dcbpy$)_2Ru(NCS)_2$. Since the electronic influence of the esterified carboxylic acid groups on the bpy ligand should be small compared to H_2-dcbpy, it can be proposed that the ester analogues can be conveniently used as superior model compounds to bpy compounds for understanding the redox and spectroscopic properties of the considerably more surface active and reactive protonated acid sensitizer compounds.[2] Commonly $[Ru(bpy)_3]^{2+}$ is taken as the model compound[5] used for comparison of electrochemical and spectroscopic data of newly synthesized ruthenium polypyridyl complexes. However, the electron withdrawing carboxylate groups present in the H_2-dcbpy and Et_2-dcbpy ligands (Et_2-dcbpy = diethyl 2,2′-bipyridine-4,4′-dicarboxylate) generate distinctively different physical and chemical properties to those of the parent bpy ligand. For example,[6–12] $[Ru(bpy)_3]^{2+}$ exhibits up to three reversible reductions and one reversible oxidation when voltammetric measurements are made under standard laboratory conditions. All reduction processes in ruthenium bipyridine complexes are considered[13] to be bipyridine based. Replacing bpy by Et_2-dcbpy to give $[Ru(Et_2$-dcbpy$)_3]^{2+}$ offers the possibility of adding up to ten electrons under voltammetric conditions to the complex and ten reversible reduction waves have been observed[11] under ultra-inert and low temperature conditions.

The electrochemical and spectroscopic properties of $[M(R_2$-bpy$)_3]^{x+}$ complexes, where R_2-bpy = bipyridine or a substituted derivative and M = Ru, Ir and Os, have been studied in great detail by DeArmond,[10–12,14–19] Elliott[20–22] and Heath and their co-workers.[8,9,23–25] A common and interesting property associated with the reduction of these polypyridine type complexes is the specific localization of added electrons on one ligand,[26] which leads to ligand based mixed valency states and induces "electron hopping"[8,27] between ligands. Surprisingly, electrochemical studies of complexes with the structure $(R_2$-bpy$)_2$-$M(X)_2$ (X = halide or pseudohalide) are only sparingly available in the literature,[28–30] although this class of complexes often exhibits different properties to the $[M(R_2$-bpy$)_3]^{x+}$ complexes, specifically in regards to oxidation and reduction processes. Additionally, to the best of our knowledge, no "electron hopping" effect has been reported for the $(R_2$-bpy$)_2M(X)_2$ class of complexes.

In previous work[31] we have investigated the oxidation of the title compounds.† In this paper, a comprehensive electrochemical and spectroscopic study is presented on the electrochemical reduction chemistry in dimethylformamide (DMF) of the system *cis*-$(Et_2$-dcbpy$)_2RuX_2$ (Et_2-dcbpy = L = diethyl 2,2′-bipyridine-4,4′-dicarboxylate, X = Cl^-, I^-, NCS^- and CN^-).

† The name given to the Et_2-dcbpy ligand previously[31] was 2,2′-bipyridine-4,4′-diethoxydicarboxylic acid. However, this name is misleading and in this paper we now use the name dimethyl 2,2′bipyridine-4,4′-dicarboxylate, which is consistent with CAS nomenclature.

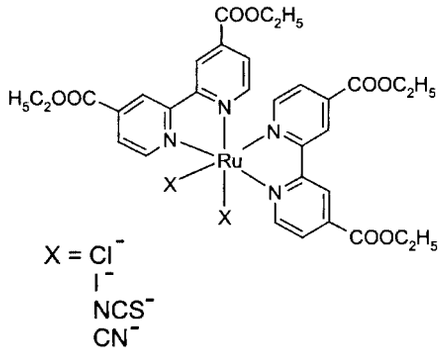

cis-L_2RuX_2

2. Experimental

Details concerning the syntheses and instrumentation used are available in reference 31. The complexes L_2RuX_2 have a *cis* configuration as determined by NMR experiments. For convenience the *cis* notation will be omitted in the remainder of the paper. All potentials are quoted *versus* the potential of the Fc^+/Fc couple, obtained from the oxidation of ferrocene (Fc) under the same experimental conditions (method, solvent, electrolyte and temperature) as the relevant experiment. In-house constructed platinum and glassy carbon macro- and micro-disk electrodes of stated diameter were used in all voltammetric experiments whilst bulk electrolysis was carried out at a platinum gauze working electrode.

HPLC grade (Mallinckrodt, UltimAR or ChromAR) dimethylformamide (DMF) containing 0.005% water content was treated with activated 3 Å molecular sieves prior to experiments to further reduce the water content. The electrolyte used for voltammetric experiments was tetrabutylammonium hexafluorophosphate (Bu_4NPF_6) which was prepared according to a literature method [32] and dried under vacuum at 90 °C for 10 hours.

3. Results and discussion

3.1. $L_2Ru(CN)_2$

(a) Voltammetry in DMF. Four very well defined processes are accessible in the voltammetric reduction of $L_2Ru(CN)_2$ at glassy carbon electrodes in DMF. Assuming the reductions are Et_2-dcbpy ligand based, then they may be formulated as follows [reactions (1)–(4)]:

$$(Et_2\text{-dcbpy})_2Ru(CN)_2 + e^- \rightleftharpoons [(Et_2\text{-dcbpy}^{\bullet -})(Et_2\text{-dcbpy})Ru(CN)_2]^- \quad (1)$$

$$[(Et_2\text{-dcbpy}^{\bullet -})(Et_2\text{-dcbpy})Ru(CN)_2]^- + e^- \rightleftharpoons [(Et_2\text{-dcbpy}^{\bullet -})_2Ru(CN)_2]^{2-} \quad (2)$$

$$[(Et_2\text{-dcbpy}^{\bullet -})_2Ru(CN)_2]^{-2} + e^- \rightleftharpoons [(Et_2\text{-dcbpy}^{\bullet -})(Et_2\text{-dcbpy}^{2-})Ru(CN)_2]^{3-} \quad (3)$$

$$[(Et_2\text{-dcbpy}^{\bullet -})(Et_2\text{-dcbpy}^{2-})Ru(CN)_2]^{3-} + e^- \rightleftharpoons [(Et_2\text{-dcbpy}^{2-})_2Ru(CN)_2]^{4-} \quad (4)$$

Fig. 1a and b show cyclic voltammograms in DMF (T = 22 °C) at a 1 mm diameter glassy carbon disk electrode at scan rates of v = 100 and 500 mV s^{-1} respectively. The first three processes [eqns. (1)–(3)] represent almost ideal models of chemically and electrochemically reversible processes, whilst the reversibility of the fourth process [eqn. (4)] depends strongly on the purity of the sample as well as on the water content of the solvent and temperature. Under optimum conditions, the fourth process was fully reversible at scan rates v > 500 mV s^{-1} at 22 °C. A voltammogram obtained under near steady-state conditions at the same electrode material but with a microdisk electrode configuration is shown in Fig. 1c and exhibits four reversible one-electron reduction steps. Cyclic voltammetric data obtained for the four processes under a range of conditions are summarized in Table 1.

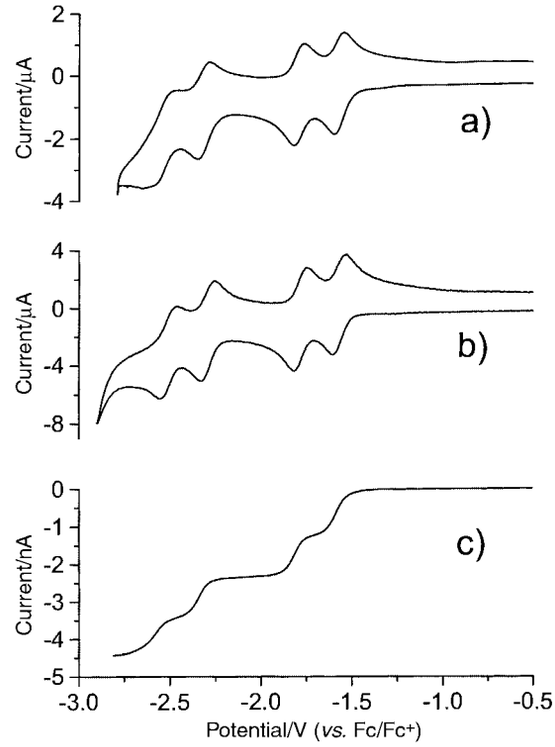

Fig. 1 Voltammetric reduction of $L_2Ru(CN)_2$ in DMF (0.1 M Bu_4NPF_6) at 22 °C: a) cyclic voltammetry, scan rate 100 mV s^{-1}, glassy carbon electrode, d = 1 mm, c = 1.1 mM; b) cyclic voltammetry, scan rate 500 mV s^{-1}, glassy carbon electrode; d = 1 mm, c = 1.1; mM; c) near steady-state conditions at a glassy carbon microdisk electrode, d = 11 μm, scan rate 10 mV s^{-1}, c = 1.7 mM.

Plots of the reduction peak height, i_p^{red}, *versus* $v^{1/2}$ from cyclic voltammograms for the first three processes are linear over the scan rate of 10 to 2000 mV s^{-1} as expected if the processes are diffusion controlled. Mass transport control was also demonstrated *via* the linear dependence of the limiting current, i_L, on the square root of the angular velocity, $\omega^{1/2}$ ($\omega = 2\pi f$, Levich plot) in rotating disk electrode experiments for the first three processes and for high rotation rates (≥1500 rpm) for the fourth process. The $E^r_{1/2}$ value (reversible half-wave potential) calculated as $(E_p^{ox} + E_p^{red})/2$ (cyclic voltammetry, with E_p^{ox} and E_p^{red} being oxidation and reduction peak potentials, respectively) and from the value of the potential at $i_L/2$ (rotating disk and microdisk electrodes) as well as other voltammetric data are given in Table 1. As required for reversible processes, the values for the initial three processes are almost independent of the voltammetric technique. Minor deviations relative to the theory for a reversible process are observed for the fourth process. The reversible half-wave potentials obtained for all four processes are summarized in Table 2.

Confirmation that the processes arise from reversible one-electron processes was obtained from plots of E *versus* $\log[(i_L - i)/i]$ ("log plots") obtained from rotating disk and microdisk electrode voltammetry, the slopes of which had values close to $2.30RT/F$ (58 mV at 22 °C), Table 1. The almost exact agreement with theory for these reversible processes under the near steady-state conditions of a microdisk electrode, compared to small departures from ideality with other techniques, implies that a small contribution from uncompensated resistance is present when the other techniques are used.

Data obtained from rotating disk electrode measurements and use of the Levich equation [33] where F is the Faraday con-

Table 1 Voltammetric data ($T = 22$ °C) for the four $L_2Ru(CN)_2$ reduction processes in DMF (0.1 M Bu_4NPF_6) at a 2 mm diameter glassy carbon electrode. $E_{1/2}$ values have an uncertainty of ±3 mV, i_p^{ox}/i_p^{red} values of ±0.04 and slopes of ±3 mV

Cyclic voltammetry				Rotating disk electrode		
v/mV s^{-1}	ΔE/mV	$E^r_{1/2}$/mV	$\lvert i_p^{ox}/i_p^{red}\rvert$	f/min^{-1}	slope/mV	$E^r_{1/2}$/mV
$[L_2Ru(CN)_2]^{0/-}$						
10	62	−1570	1.06	500	74	−1573
26	60	−1571	1.03	1000	77	−1573
50	71	−1574	1.02	1500	80	−1573
100	74	−1572	1.04	2000	84	−1574
200	88	−1574	0.98	2500	83	−1579
500	108	−1571	1.01	3000	86	−1579
1000	132	−1571	1.06			
2000	154	−1574	1.00	Microdisk electrode		
				r/μm	slope/mV	$E^r_{1/2}$/mV
				5.6	64	−1569
$[L_2Ru(CN)_2]^{-/2-}$						
10	58	−1792	1.07	500	62	−1814
26	59	−1793	1.00	1000	68	−1815
50	71	−1794	0.96	1500	66	−1820
100	69	−1794	0.93	2000	65	−1827
200	82	−1794	0.97	2500	66	−1833
500	106	−1792	0.91	3000	60	−1836
1000	128	−1795	0.93			
2000	170	−1799	1.01	Microdisk electrode		
				r/μm	slope/mV	$E^r_{1/2}$/mV
				5.6	58	−1797
$[L_2Ru(CN)_2]^{2-/3-}$						
10	70	−2320	1.08	500	71	−2353
26	84	−2321	1.07	1000	64	−2353
50	90	−2324	1.04	1500	65	−2363
100	90	−2322	1.07	2000	64	−2377
200	105	−2321	1.04	2500	58	−2382
500	106	−2320	1.00	3000	57	−2394
1000	128	−2321	0.98			
2000	178	−2330	1.03	Microdisk electrode		
				r/μm	slope/mV	$E^r_{1/2}$/mV
				5.6	58	−2326
$[L_2Ru(CN)_2]^{3-/4-}$						
10	90	−2520		500	67	−2582
26	74	−2528		1000	67	−2608
50	70	−2530		1500	66	−2633
100	82	−2532		2000	78	−2645
200	106	−2538		2500	—	—
500	120	−2547		3000	—	—
1000	144	−2549				
2000	196	−2549		Microdisk electrode		
				r/μm	slope/mV	$E^r_{1/2}$/mV
				5.6	69	−2555

$$i_L = 0.620FAD^{2/3}\omega^{1/2}k^{-1/6}c_0 \quad (5)$$

stant, c_0 is the bulk concentration, ω is the angular velocity ($2\pi f$), k is the kinematic viscosity of the solvent and D the diffusion coefficient, enabled the diffusion coefficient to be calculated with a value of $D = 3.0(\pm 0.4) \times 10^{-6}$ cm^2 s^{-1}. From data obtained from microelectrode voltammograms and use of the relationship $i_L = 4nFrc_0D$ (r = electrode radius) an average diffusion coefficient of $D = 2.9(\pm 0.2) \times 10^{-6}$ cm^2 s^{-1} can be calculated. These diffusion coefficients are in excellent agreement with the value of $D = 3.1(\pm 0.2) \times 10^{-6}$ cm^2 s^{-1} measured by using the oxidation process.[31]

(b) Temperature dependence. An interesting thermodynamic effect was observed when voltammetric data obtained at 22 °C were compared to data obtained at −58 °C (close to the freezing point of DMF which is −61 °C). At 22 °C, the reversible $E^r_{1/2}$ values for the first pair of processes are separated

Table 2 Reversible half-wave potentials for the reduction of L_2RuX_2 in DMF (0.1 M Bu_4NPF_6)

Complexes	Reversible potentials[a] $E^r_{1/2}$/mV			
	$[L_2RuX_2]^{0/-}$	$[L_2RuX_2]^{-/2-}$	$[L_2RuX_2]^{2-/3-}$	$[L_2RuX_2]^{3-/4-}$
$L_2Ru(CN)_2$	−1570 ± 3	−1796 ± 5	−2326 ± 7	−2550 ± 20
$L_2Ru(NCS)_2$	−1480 ± 3	−1697 ± 4	−2230 ± 20	−2428 ± 6[b]
L_2RuI_2	−1555 ± 10	—	—	—
L_2RuCl_2	−1588 ± 4	−1790 ± 10[b]	—	—

[a] mV *versus* Fc/Fc^+. [b] $T = -58$ °C, other data reported at $T = 22$ °C.

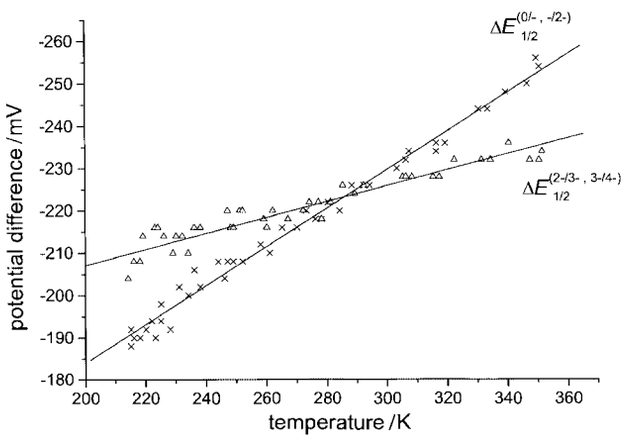

Fig. 2 Temperature dependence of the $E_{1/2}$ separation for the first and second pairs of reduction processes for $L_2Ru(CN)_2$. First pair: $\times\cdots\Delta E^{(0/-,-/2-)}_{1/2}$, second pair: $\Delta\cdots\Delta E^{(2-/3-,3-/4-)}_{1/2}$.

by $\Delta E^{(0/-,-/2-)}_{1/2} = -226$ mV and the second pair of processes by $\Delta E^{(2-/3-,3-/4-)}_{1/2} = -224$ mV. However, the separations were significantly smaller at −58 °C. Peak potentials obtained from differential pulse voltammetry were used to determine these $\Delta E^r_{1/2}$ values over the temperature range from −60 to +80 °C and a linear dependence on temperature was found for both $\Delta E^{(0/-,-/2-)}_{1/2}$ and $\Delta E^{(2-/3-,3-/4-)}_{1/2}$ (Fig. 2 and Table 3). However, interestingly, since the slopes for both pairs of reduction processes are different, a crossover occurs at $T = 15 \pm 15$ °C. The data measured for the second set of reduction processes contain an error, since the fourth process is not fully reversible in the higher temperature range. However, this error must be small since under conditions where this process is fully reversible (*i.e.* $T < 0$ °C) the same linear relationship is found as also is the case when rotating disk electrode voltammetry and cyclic voltammetry at moderately fast scan rates ($v = 1000$ mV s^{-1}) are used to calculate $E^r_{1/2}$ values.

The observation that the $\Delta E_{1/2}$ value for the first set of reduction processes is smaller than that for the second set of processes, as observed in this study on $L_2Ru(CN)_2$ at temperatures <15 °C, has been commonly explained in terms of the overall charge of the complex; the higher the overall charge of the complex, the higher the energy needed to add an additional charge. Although no discussion concerning the opposite potential separation found at higher temperatures in this work appears to be available in the literature, there are related systems which may be examined in this context. For $[Ru(bpy)_3]^{2+}$ and $[Ru(Et_2\text{-dcbpy})_3]^{2+}$, voltammetric data for the reduction processes in DMF at +20 °C [21] and −54 °C [11] have been reported. Unfortunately, the accuracy of the reported potential values (±5 mV) only allows qualitative comparison to be made for both compounds. In the case of $[Ru(bpy)_3]^{2+}$, the first set of reduction processes yield $\Delta E^{(2+/+,0/-)}_{1/2} = -0.43$ V at 20 °C and −0.38 V at −54 °C. For $[Ru(Et_2\text{-dcbpy})_3]^{2+}$ $\Delta E^{(2+/+,0/-)}_{1/2} = -0.30$V at 20 °C and −0.28 V at −54 °C whereas $\Delta E^{(-/2-,3-/4-)}_{1/2} = -0.52$ V at 20 °C and −0.43 V at −54 °C. Apparently the latter compound exhibits a stronger temperature dependence for the second set of reduction processes than $L_2Ru(CN)_2$, which in contrast shows a stronger temperature dependence for the first set of reductions.

Table 3 $\Delta E_{1/2}$ data obtained by least squares linear regression of plots of potential separations of indicated reduction processes *versus* temperature (r = correlation coefficient)

Complex	Process	Intercept/ mV	Slope/ mV K^{-1}	r(%)
$L_2Ru(CN)_2$	$\Delta E^{(0/-,-/2-)}_{1/2}$	−92	−0.46	99.3
	$\Delta E^{(2-/3-,3-/4-)}_{1/2}$	−169	−0.19	95.5
$L_2Ru(NCS)_2$	$\Delta E^{(0/-,-/2-)}_{1/2}$	−98	−0.42	99.3

The linear relationship between temperature and potential (energy) for $\Delta E_{1/2}$ values may be explained in terms of entropy. By assuming that $E_{1/2} = E^r_{1/2} = E^{0\prime}$ ($E^{0\prime}$ = formal potential), the relationship between the measured $E_{1/2}$ and the Gibb's free energy, and hence entropy, is given by

$$E_{1/2} = -\frac{\Delta G}{nF} = \frac{\Delta H - T\Delta S}{nF} \quad (6)$$

where $\Delta S = S^- - S^0$ (S^0 and S^- being the entropies of $[L_2Ru(CN)_2]^0$ and $[L_2Ru(CN)_2]^-$, respectively) and $n = 1$ for the $[L_2Ru(CN)_2]^{0/-}$ process. Thus, $\Delta E^{(0/-,-/2-)}_{1/2}$ can be formulated as

$$\Delta E^{(0/-,-/2-)}_{1/2} = \frac{\Delta\Delta H - T(S^{2-} + S^0 - 2S^-)}{F} \quad (7)$$

where $\Delta\Delta H$ is the difference between the enthalpy changes in both processes and S^{2-} is the entropy of $[L_2RuX_2]^{2-}$. Assuming a localized electron model, in the one-electron reduced species, $[L_2RuX_2]^-$, the electron can "hop" between the ligands. This hopping can be considered to provide an additional degree of freedom which can be expressed as an additional entropy term. The two electron reduced form, $[L_2RuX_2]^{2-}$, which has both Et_2-dcbpy ligands filled up with an electron, and L_2RuX_2 lack this ability to permit electron hopping, and hence lack the additional entropy term. In this simplified model, the entropy of $[L_2RuX_2]^-$ may be written as

$$S^- = S_{system} + S^-_{electron\ hopping} \quad (8)$$

where additional entropy differences between both redox states, for example due to different solvation entropies, are neglected. Thus, using this approximate theory, the entropy for L_2RuX_2 and $[L_2RuX_2]^{2-}$ is only

$$S^0 = S^{2-} = S_{system} \quad (9)$$

and eqn. (7) reduces to

$$\Delta E^{(0/-,-/2-)}_{1/2} = \frac{\Delta\Delta H - T2S^-_{electron\ hopping}}{F} \quad (10)$$

so that $\Delta E^{(0/-,-/2-)}_{1/2}$ is governed by the magnitude of $S^-_{electron\ hopping}$. Assuming ΔH is independent of temperature for all the processes yields a linear relationship of $\Delta E_{1/2}$ with T with a

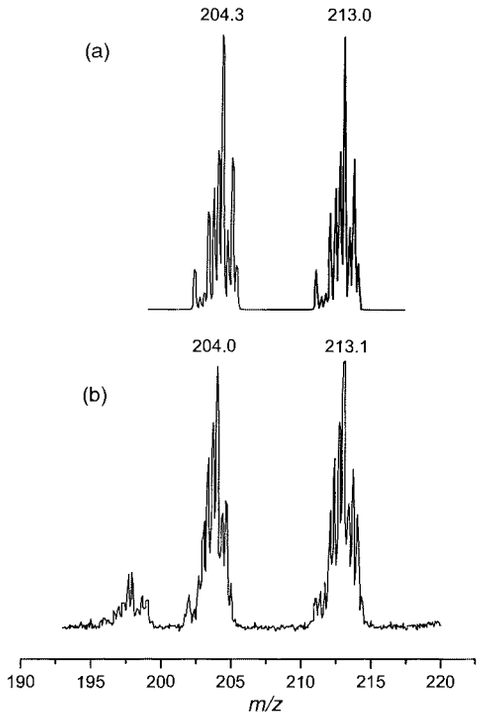

Fig. 3 Negative ion mode electrospray mass spectrum of a) exhaustive bulk electrolyzed solution of 1.0 mM $L_2Ru(CN)_2$ at $E_{appl} = -2.0$ V in DMF (0.01 mM Bu_4NPF_6), b) simulation of mass spectra for $[\{(^-OOC)_2bpy\}_2Ru(CN)]^{3-}$, $m/z = 204.3$, and $[\{(^-OOC)_2bpy\}_2Ru(CN)_2]H^{3-}$, $m/z = 213.0$.

slope of $-2S^{-}_{\text{electron hopping}}/F$. Analogous arguments apply for the second $\Delta E^{(2-/3-,3-/4-)}_{1/2}$ value, which is governed by the magnitude of $S^{3-}_{\text{electron hopping}}$. The different dependences of $\Delta E_{1/2}$ on T imply that $S^{-}_{\text{electron hopping}}$ and $S^{3-}_{\text{electron hopping}}$ have different values. This localized electron model leads to the prediction that, since $[L_2RuX_2]^-$ and $[L_2RuX_2]^{3-}$ have an additional electron hopping term, they are in a preferred lower energetic state. That is, the reduction of L_2RuX_2 to the one-electron reduced form and the reduction of $[L_2RuX_2]^{2-}$ to $[L_2RuX_2]^{3-}$ therefore occur more readily and hence at a more positive potential than would be the case without the additional entropy term.

(c) Bulk electrolysis at 22 °C and examination of reduction products by electrospray mass spectrometry. Although the first two reduction processes were found to be chemically and electrochemically fully reversible at 22 °C under voltammetric time scales, reduced temperatures were necessary to quantitatively generate $[L_2Ru(CN)_2]^-$ and $[L_2Ru(CN)_2]^{2-}$ [eqn. (1) and (2)] under conditions of controlled potential bulk electrolysis (*vide infra*). The technique of electrospray mass spectrometry (ESMS) was employed to identify decomposition pathways that occur on longer time scales.

In one bulk electrolysis experiment, a 0.6 mM solution of $L_2Ru(CN)_2$ in DMF (0.01 M Bu_4NPF_6) was exhaustively electrolyzed at 22 °C. The controlled potential was set at a value slightly more negative than the second reduction process (−2.05 V *vs.* Fc/Fc^+) using a large surface area platinum gauze working electrode. The electrospray mass spectrum of the nominally two-electron bulk electrolyzed solution of $L_2Ru(CN)_2$ (Fig. 3) in the negative ion mass spectrum detection mode over the range 150–1200 *m/z* revealed only two major ruthenium products. Simulation (Fig. 3b) enabled the products to be identified as the fully de-esterified and deprotonated acid $[\{(COO^-)_2\text{-bpy}\}_2Ru(CN)_2]^{4-}$, detected as the singly protonated form $[\{(COO^-)_2\text{-bpy}\}_2Ru(CN)_2]H^{3-}$, which has a −3 overall charge at 213 *m/z*. The second signal at 204 *m/z*, also having a −3 charge, can be identified as the fully de-esterified and deprotonated acid $[\{(COO^-)_2\text{-bpy}\}_2Ru(CN)]^{3-}$ which also has lost one cyanide ligand. If the bulk electrolysis potential is set after the first process at $E_{appl} = -1600$ mV, only mixtures of partially de-esterified starting compound are observed in the mass spectra. That is, evidence for reductively eliminated cyanide could only be found in solutions exhaustively electrolyzed at potentials more negative than the second process. No signals due to ruthenium compounds were found in the positive ion detection mode.

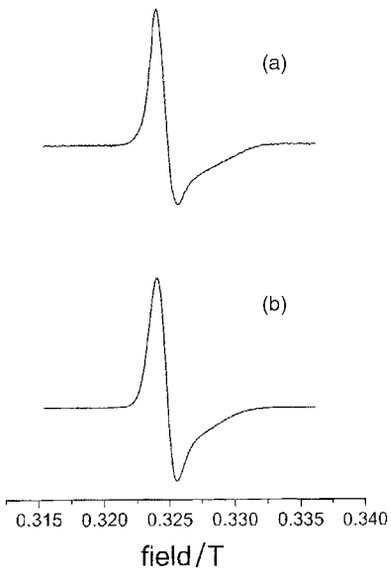

Fig. 4 ESR spectra of $[L_2Ru(CN)_2]^-$: a) in DMF glass at 77 K, b) spectrum simulated with parameters given in Table 4.

The bulk electrolysis reduction ESMS detection experiments suggest that after the one-electron reduction of $(Et_2\text{-dcbpy})_2Ru(CN)_2$ to $[(Et_2\text{-dcbpy})_2Ru(CN)_2]^-$ at 22 °C in DMF, loss of the ester groups occurs, whilst after further exhaustive reduction of the solution reductive elimination of one cyanide ligand occurs. Both classes of reaction are documented in the literature. For example, aromatic esters of pyridine derivatives have been shown[34–37] to produce the deprotonated acid analogues when electrochemically reduced in organic solvents and with related $(bpy)_2RuX_2$ systems[28] loss of X^- has been observed when the complex was reduced. Further proof for these reactions pathways will be presented later in this paper.

(d) ESR measurements on $L_2Ru(CN)_2$ reduced at −55 °C. The one- and two-electron reduced $L_2Ru(CN)_2$ complexes were prepared *ex situ* by bulk electrolysis at −55 °C in DMF. Steady-state voltammetric measurements undertaken during the course of the reduction indicated that conversion of the desired product back to the starting material occurred during bulk electrolysis experiments, as would be expected if the two electron reduced compound can catalytically reduce residual water or even the electrolyte or solvent to yield a less reduced form.[38,39] This resulted in more charge being consumed than theoretically predicted. The ESR spectrum of the pure singly reduced $[L_2Ru(CN)_2]^-$ in DMF glass at 77 K is shown in Fig. 4 and may been seen to exhibit a single signal at $g_\perp = 2.000$ with a broad wing at the higher field side which is due to the superimposed parallel component $g_\parallel = 1.980$. The ESR spectrum is similar to that reported for $[Ru(bpy)_3]^+$.[12] Diminished signal intensities at elevated temperatures (>180 K) prevented the detection of temperature dependent line broadening as frequently observed for similar compounds[10,12,18,19,27,40] and attributed to "electron hopping" between ligands.

Owing to reactions with residual water (see above), only solutions of partly two-electron reduced $L_2Ru(CN)_2$ (30–50% $[L_2Ru(CN)_2]^{2-}$ content) could be prepared by bulk electrolysis. The ESR spectra obtained from impure solutions

Table 4 Spectroscopic data for L_2RuX_2 and reduced forms of L_2RuX_2 in DMF: a) electronic spectral data obtained for reduced forms of $L_2Ru(CN)_2$ at −58 °C, b) electronic spectral data obtained for L_2RuX_2 complexes at 22 °C, c) parameters used for simulation of the ESR spectrum shown in Fig. 4

a)		Absorbance						
	Complex	Energy/10^3 cm^{-1} (Molar absorption/10^3 mol^{-1} cm^{-1})						
	$[(L^{\bullet -})LRu(CN)_2]^-$	31.5 (40.0)	27.7 (20.0)	22.3 (17.7)	18.2 (15.5)	17.0 (10.7)	6.0 (5.3)	3.5 (0.8)
	$[(L^{\bullet -})Ru(CN)_2]^{2-}$	—	27.5 (42.2)	20.5 (21.5)			5.7 (11.4)	—

b)		MLCT	MLCT
	$L\pi \longrightarrow L\pi^*$	$Md_\pi \longrightarrow L\pi_2^*$	$Md_\pi \longrightarrow L\pi_1^*$
	Energy/10^3 cm^{-1} (Molar absorption/10^3 mol^{-1} cm^{-1})		
L_2RuCl_2	31.1 (37.4)	23.1 (13.1)	16.9 (14.2)
L_2RuI_2	31.2 (39.0)	23.5 (13.6)	17.2 (12.9)
$L_2Ru(NCS)_2$	31.3 (45.7)	24.5 (14.3)	18.1 (14.5)
$L_2Ru(CN)_2$	31.5 (58.4)	25.0 (18.0)	18.8 (22.1)

c)	$g_\perp$ (ΔH/mT)	$g_{\text{parallel;}}$ (ΔH/mT)
$[(L^{\bullet -})LRu(CN)_2]^-$	1.9996 (1.3)	1.9800 (3.6)
$[(L^{\bullet -})LRu(NCS)_2]^-$		

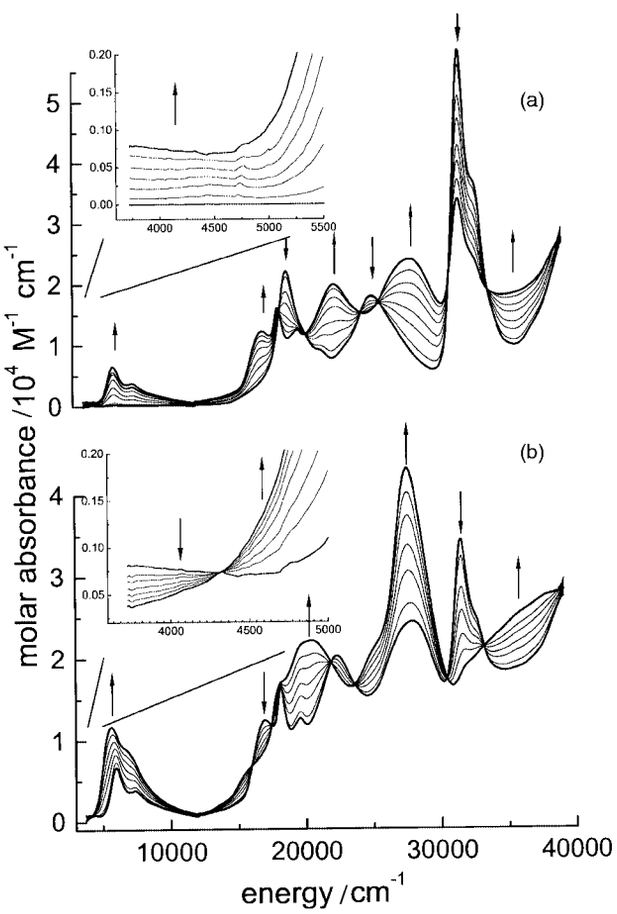

Fig. 5 Electronic spectra obtained in an OTTLE cell during the course of reduction of 0.6 mM $L_2Ru(CN)_2$ in DMF (0.2 M Bu_4NPF_6) at −58 °C: a) reduction of $L_2Ru(CN)_2$ to $[L_2Ru(CN)_2]^-$, b) reduction to $[L_2Ru(CN)_2]^{2-}$. Inserts show evidence for a weak NIR band for the one-electron reduced form.

of $[L_2Ru(CN)_2]^{2-}$ were undistinguishable from that of $[L_2Ru(CN)_2]^-$ except for the fact that the intensity of the signal was enhanced.

(e) Spectroelectrochemical studies on reduced $L_2Ru(CN)_2$. Electronic spectra of the one- and two-electron reduced forms of $L_2Ru(CN)_2$ can be obtained at −58 °C in DMF (Fig. 5) *via in situ* OTTLE spectroelectrochemical experiments. These low temperature, small volume (0.5–1.5 ml) and relatively short time domain OTTLE experiments enabled the two-electron reduced form of $L_2Ru(CN)_2$ to be generated almost quantitatively. Reduction to $[L_2Ru(CN)_2]^-$ and re-oxidation back to the starting material occurred without any detectable loss of material in the sense that the initial and final electronic spectra were identical. Analogous experiments associated with generation of $[L_2Ru(CN)_2]^{2-}$ and re-oxidation back to the starting material showed losses of material of less than 5%. Owing to the considerable richness of the electronic spectra of both reduced and oxidized forms of the compounds at least six isosbestic points emerge during the course of reduction of $L_2Ru(CN)_2$ to $[L_2Ru(CN)_2]^-$ and seven for the additional reduction to $[L_2Ru(CN)_2]^{2-}$.

Electronic spectral data are summarized in Table 4. The spectra of the reduced compounds reflect the occurrence of Et_2-dcbpy ligand based reductions. In the case of $[Ir(bpy)_3]^{3+}$ and $[Ru(bpy)_3]^{2+}$, it has been elegantly shown [9,24,26] that the electronic spectra of the triply reduced forms are almost identical with the spectrum of the one-electron reduced free ligand. In this sense, the reduction from $[L_2Ru(CN)_2]^-$ to $[L_2Ru(CN)_2]^{2-}$ leads to the complete disappearance of the characteristic Et_2-dcbpy ligand $\pi \longrightarrow \pi^*$ band at 31500 cm^{-1}. Additionally, both MLCT bands present at 25000 and 18800 cm^{-1} disappear, whilst new intraligand bands grow in in the same region. The spectrum of $[L_2Ru(CN)_2]^-$ is complicated in the visible region by superimposition of the Ru^{II}–$(Et_2$-dcbpy$)^0$ MLCT and the characteristic Et_2-dcbpy^{-1} intraligand transitions. The spectrum of $[L_2Ru(CN)_2]^{2-}$ resembles that of reduced bipyridine,[26,41] the major difference being the position of an intense NIR band at 5700 cm^{-1} occurring at significantly lower energies than in bpy$^-$ and $[Ru(bpy)_3]^-$ (≈12500 cm^{-1}). The large shift of this NIR band relative to that of bpy reflects the substantially different energies of the molecular orbitals of the ligands and especially the differences in relative orbital energies as determined by MNDO calculations.[16] The calculated energy difference between the π_1^* and π_2^* orbitals is approximately halved when comparing Et_2-dcbpy and bpy, as is also the case with the energy of this experimentally observed band. Consequently, this transition is tentatively assigned as arising from an Et_2-dcbpy based $\pi_1^* \longrightarrow \pi_2^*$ transition. This is consistent with Elliott's observation that this band disappears when a second electron is placed onto the ligand, which will significantly lower the π_1^* energy and hence shift the band out of that region. On the basis of the above argument, the shoulder at *ca.* 7400 cm^{-1} will then be due to a $\pi_1^* \longrightarrow \pi_3^*$ transition, as the π_2^* and π_3^* orbitals are almost identical in energy.

The band for $[L_2Ru(CN)_2]^-$ in the near infrared region at ≈3500 cm^{-1}, having a very low absorbance (see Fig. 5 inserts), is attributable to an inter-ligand inter-valence charge transfer (IVCT), first reported for the $[Ru(bpy)_3]^{2+}$ system by Heath and co-workers.[8] Its presence provides further evidence of inter-ligand electron hopping. Unfortunately, solvent overtones and strong absorbance from residual water mask this process. However, data points obtained at lower energies enabled the position and peak intensity to be estimated by interpolation. This transition is caused by electron hopping[8,27] from one Et_2-dcbpy ligand to the other as described in eqn. (11). As expected, this

$$[(L^{\bullet -})(L)RuX_2]^- + h\nu \longrightarrow [(L)(L^{\bullet -})RuX_2]^- \quad (11)$$

band disappears when $[L_2Ru(CN)_2]^-$ is reduced to $[L_2Ru(CN)_2]^{2-}$ and this feature leads to an additional isosbestic point, as shown in the relevant insert in Fig. 5. The position of this band is similar to that of reduced $[Ru(bpy)_3]^{2+}$ (4500 cm^{-1}),[8] although the absorbance is about three times higher (see Table 4).

In recent papers[42,43] the authors of pump and probe laser experiments reported an estimate of the electron injection rate of excited $(H_2\text{-dcbpy})_2Ru(NCS)_2$ into TiO_2. The probing was undertaken at wavelengths of 750 and 1100 nm, which were thought to be typical of the oxidized dye $[(H_2\text{-dcbpy})_2Ru(NCS)_2]^+$ and hence indicative of the rate of arrival of the electron into the semiconductor. The calculated rates implied that electron injection is faster than the detector response time. Interestingly, spectra for the reduced forms of $L_2Ru(CN)_2$ (Fig. 5), which are expected to be very similar to that of reduced $(H_2\text{-dcbpy})_2Ru(NCS)_2$, show very strong absorbances at the same wavelength regions where the probing was undertaken in these experiments. These bands, assigned in this work to intra-ligand charge transfers in the reduced form of the ligand, therefore also are expected to be present in the excited state, which formally has the configuration $[(L^{\bullet -})(L)Ru^+X_2]$. Thus, it is likely that the formation of the excited state rather than the electron injection time has been measured in the work of references 42 and 43. Authors of a recent paper[44] recognized this problem and have used mid-IR frequencies (4–7 μm) to directly probe conduction band electrons.

3.2 $L_2Ru(NCS)_2$

(a) Voltammetry in DMF. A cyclic voltammogram for reduction of $L_2Ru(NCS)_2$ is shown in Fig. 6a and can be seen to exhibit many of the characteristics found for the cyanide analogue. The main difference is the decreased stability of the reduced forms. For this compound, only the first two reduction processes are chemically and electrochemically reversible at 22 °C. Under conditions of cyclic voltammetry, i_p^{red} for the first two processes scaled linearly with $\nu^{1/2}$ and a Levich plot (rotating disk electrode) was linear and passed through the origin for both processes, establishing that both processes are mass transport controlled. $E^r_{1/2}$ values for both processes obtained from these two techniques were calculated to be -1480 ± 3 mV and -1697 ± 4 mV *vs.* Fc/Fc^+ and coincided with values obtained from microdisk electrode experiments under near steady-state conditions. "Log-plots" from microdisk and rotating disk electrode voltammograms gave slopes of 63 ± 3 mV, which are close to the theoretical value expected for a reversible one-electron process. Slopes of rotating disk electrode Levich plots for the first and second processes were identical within experimental error and lead to a diffusion coefficient for $L_2Ru(NCS)_2$ in DMF of $D = 3.2 \pm 0.4 \times 10^{-6}$ cm^2 s^{-1}, which is very similar to the value obtained for $L_2Ru(CN)_2$. Cyclic voltammetric scan rates >200 mV s^{-1} were required to make the third reduction process of $L_2Ru(NCS)_2$ fully reversible. Under near steady-state conditions of a microdisk electrode, and also in rotating disk electrode experiments, the third process appears to be reversible in the sense that slopes calculated from "log-plots" were 61 ± 5 mV, close to the value of 58 mV theoretically expected for a reversible one-electron process. $E^r_{1/2}$ values calculated from these "log-plots" for the third process were in agreement with those obtained from cyclic voltammograms ($\nu > 200$ mV s^{-1}). Thus the reversible half-wave potential for the $[L_2Ru(NCS)_2]^{2-/3-}$ process is established to be -2230 ± 20 mV.

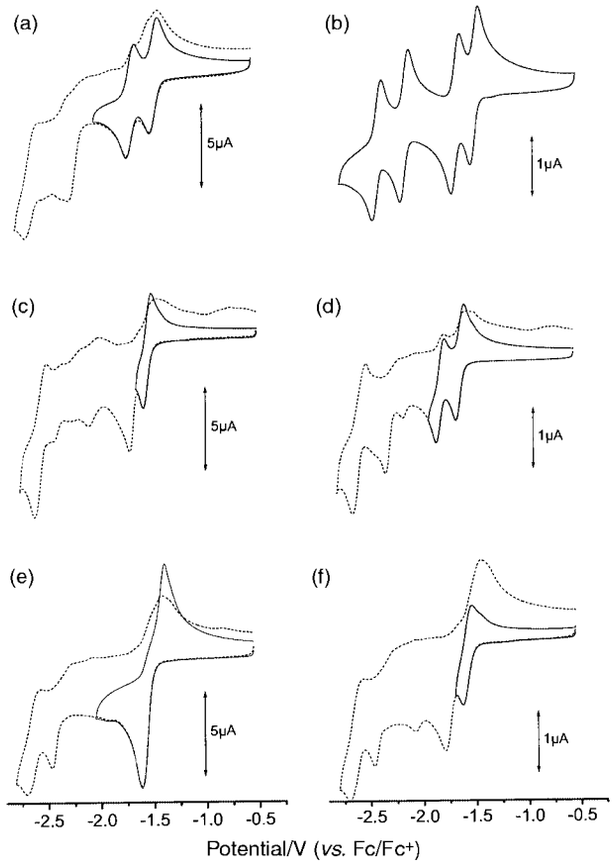

Fig. 6 Cyclic voltammograms for reduction of L_2RuX_2 as a function of switching potential and temperature in DMF (0.1 M Bu_4NPF_6) at a glassy carbon working electrode ($d = 1.5$ mm, $\nu = 100$ mV s^{-1}). 1.0 mM $L_2Ru(NCS)_2$, a) $T = 22$ °C, b) $T = -58$ °C; 1.0 mM L_2RuCl_2, c) $T = 22$ °C, d) $T = -58$ °C; 1.1 mM L_2RuI_2, e) $T = 22$ °C, f) $T = -58$ °C.

At temperatures below −20 °C, the third and fourth processes become fully reversible (Fig. 6b) under all voltammetric conditions. The reversible half-wave potentials at −58 °C for the third and fourth process were measured to be -2160 ± 6 mV and -2428 ± 6 mV *vs.* Fc^+/Fc in DMF. As was the case with $L_2Ru(CN)_2$, the reversible half-wave potentials of the reduction processes were investigated as a function of temperature. Owing to the low reversibility of the third and fourth processes at elevated temperatures only the first two processes were investigated. $\Delta E^{(0/-,-/2-)}_{1/2}$ was again found to vary in a linear manner with temperature over the temperature range −60 to +80 °C, the slope being similar to that obtained with $L_2Ru(CN)_2$ (see Table 2).

(b) Bulk electrolysis and ESR spectra. To generate the singly reduced $[L_2Ru(NCS)_2]^-$ anion, controlled potential bulk electrolysis of a 1.0 mM solution of $L_2Ru(NCS)_2$ in DMF (0.1 M Bu_4NPF_6) was carried out at $E_{appl} = -1550$ mV and $T = -58$ °C. The reduced stability of reduced forms of $L_2Ru(NCS)_2$ compared to $L_2Ru(CN)_2$ did not allow the electrolysis to go to completion without product decomposition. Therefore samples for ESR measurements were collected after ≤0.5 electrons per molecule had been transferred to ensure that no appreciable decomposition of $[L_2Ru(NCS)_2]^-$ had taken place. The ESR signal of $[L_2Ru(NCS)_2]^-$ in DMF glass at 77 K was indistinguishable from that of $[L_2Ru(CN)_2]^-$.

3.3. L_2RuI_2 and L_2RuCl_2

(a) Voltammetry and reductively induced halide ligand elimination. At 22 °C and under conditions of cyclic voltammetry at a scan rate of 100 mV s^{-1} (Fig. 6c), L_2RuI_2 is irreversibly rather than reversibly reduced (peak potential: −1630 mV). Under these conditions, the first two reduction processes expected on the basis of data obtained with the cyanide and thiocyanate derivatives have merged into a single irreversible process. Lowering the temperature to −58 °C increases the reversibility of the first two reduction processes and simplifies the voltammogram (Fig. 6f). At this low temperature, the first reduction process is chemically and electrochemically fully reversible under the near steady-state conditions of the microdisk or rotating disk electrode and under conditions of cyclic voltammetry at scan rates ≥100 mV s^{-1}. As expected, the measured $E^r_{1/2}$ value (see Table 2) was technique independent. Slopes of "log-plots" obtained from steady-state voltammograms were 42 ± 4 mV as theoretically expected (43 mV at −58 °C) for a one-electron process. Only a peak potential of $E_p^{red} = -1720$ mV ($v = 100$ mV s^{-1}, cyclic voltammetry) can be quoted for this second irreversible process under the low temperature voltammetric conditions used.

Slow scan rate cyclic voltammograms of L_2RuCl_2 at 22 °C reveal the presence of one partly reversible reduction process (Fig. 6c), followed by a series of irreversible processes. At scan rates ≥200 mV s^{-1} the first reduction process was close to reversible and the $E_{1/2}$ value calculated as $(E_p^{ox} + E_p^{red})/2$ was constant (±3 mV) over the scan rate range of 25 to 2000 mV s^{-1}, which implies that this value is close to the reversible $E^r_{1/2}$ value. Slopes calculated from "log-plots" obtained from near steady-state microdisk electrode and rotating disk electrode voltammograms were 62 ± 3 mV and $E^r_{1/2}$ values obtained from the latter techniques coincided with the value obtained from cyclic voltammograms (Table 2). Again at reduced temperature, the chemical reversibility of this system increased. At −58 °C the first reduction process is fully reversible even at slow scan rates (Fig. 6e) whilst the second reduction process becomes partly reversible. The low temperature reversible $E^r_{1/2}$ value for this second process is listed in Table 2.

Cyclic voltammograms for L_2RuI_2 in DMF in the positive potential region before and after the potential is scanned over the first reduction wave are shown in Fig. 7b. On the second cycle, two new oxidative processes appear if the reductive process is included in the initial scan. The first of these new processes precedes the metal centered oxidation of L_2RuI_2 ($E_p^{ox} = +0.05$ V) and is due to the oxidation of liberated I^-, whilst the second of the new processes, which follows the metal centered oxidation of L_2RuI_2, is attributable to the reversible one-electron oxidation of $[L_2RuI(DMF)]^+$.[31] The major difference between oxidatively[31] and reductively induced ligand elimination (this work) is the oxidation state of the eliminated ligand. Thus, chemically irreversible oxidation eliminates the oxidized ligand (I_2), whilst irreversible reduction eliminates the reduced form of the ligand (I^-).

The potential of the $[L_2RuI(DMF)]^{+/2+}$ couple at $E_{1/2} = +0.45$ V *vs.* Fc/Fc^+ is in very good agreement with the value $E_{1/2} = +0.46$ V *vs.* Fc/Fc^+ obtained from electrochemically generated solutions of $[L_2RuI(DMF)]^+$.[31] Slower scan rates reveal the appearance of the bis-solvent $[L_2Ru(DMF)_2]^{2+}$ complex in the positive potential range. Reversible oxidation for the $[L_2Ru(DMF)_2]^{3+/2+}$ couple occurs at $E_{1/2} = +0.62$ V *vs.* Fc/Fc^+, which agrees with $E_{1/2} = +0.62$ V *vs.* Fc/Fc^+ for this process when using electrochemically generated solutions of $[L_2Ru(DMF)_2]^{2+}$.[31]

The analogous behavior observed for L_2RuCl_2 is shown in Fig. 7a. In this compound, chloride is lost after the potential is scanned over the first two reduction waves and the formation of the mixed solvent complex is seen when the potential is scanned back to the positive potential region. Slower scan rates reveal

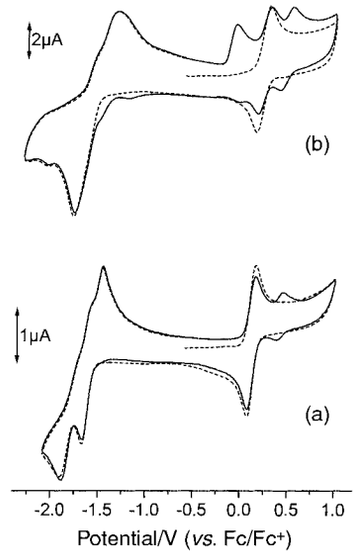

Fig. 7 First (dashed) and second cycles (full line) of cyclic voltammograms for reduction of a) 1.0 mM L_2RuCl_2 in DMF (0.1 M Bu_4NPF_6) at a 1 mm diameter platinum electrode, $v = 100$ mV s^{-1}, b) 1.0 mM L_2RuI_2 in DMF (0.1 M Bu_4NPF_6) at a 1 mm diameter glassy carbon working electrode, $v = 500$ mV s^{-1}.

the appearance of the bis-solvent $[L_2Ru(Solvent)_2]^{2+}$ complex and the reaction details are summarized in eqn. (12)–(14).

$$L_2Ru^{II}X_2 + e^- \rightleftharpoons [(L^{\bullet -})(L)Ru^{II}X_2]^- \quad (12)$$

$$[(L^{\bullet -})(L)Ru^{II}X_2]^- \longrightarrow (L^{\bullet -})(L)Ru^{II}X(Solvent) + X^- \quad (13)$$

$$(L^{\bullet -})(L)Ru^{II}X(Solvent) + Solvent \longrightarrow [(L^{\bullet -})(L)Ru^{II}(Solvent)_2]^+ + X^- \quad (14)$$

In contrast, reduced forms of $L_2Ru(CN)_2$ and $L_2Ru(NCS)_2$, which are much more stable, did not give rise to formation of these solvent complexes on the time scale of cyclic voltammetry. Even scanning up to the cathodic solvent limit did not generate any additional process(es) corresponding to oxidation of the pseudohalide/solvent mixed complex at positive potentials on the second cycle. This difference in stability of the reduced complexes can be explained by the capability of the isothiocyanate and cyanide ligand to establish strong π-back-bonding, which may compensate for the loss in σ-bonding that occurs on reduction. That is, the ability to maintain a strong π-back-bond determines the stability of L_2RuX_2 (L = bipyridine, X = halide or pseudohalide) bipyridine based reduction products.

The origin of the decreased stability of reduced forms of L_2RuX_2 where X=Cl, I compared to X = CN, NCS may be understood in terms of molecular orbital considerations. Cyanide and isothiocyanate are both good σ-donors as well as π-acceptors. In contrast, chloride and iodide are not capable of maintaining a strong π-back-bond. After the Et_2-dcbpy π* orbital is occupied upon reduction, the bipyridine will lose its ability to adequately stabilizing the dπ metal orbitals and thereby maintain a strong dπ–π* back-bond. On the other hand, the σ-donor strength increases, and indeed, in many cases, the reduced forms of aromatic imine ligands have been found[45] to be better ligands than the unreduced ligands. This increased σ-donor strength lowers the energy of the dσ orbitals of the ruthenium metal which will then affect the σ-bond strength of other ligands, which can lead to a loss of unreduced ligand, partly because of the *trans* effect.[46] An alternative explanation is based on the tendency of compounds to reach a state of minimal charge. Accordingly in this context, the complex frees itself from the additional charge imposed by the reduction process, by ejecting an anionic ligand. In $(bpy)_2RuX_2$ systems,[28] the loss of X^- also occurred when the complex was reduced.

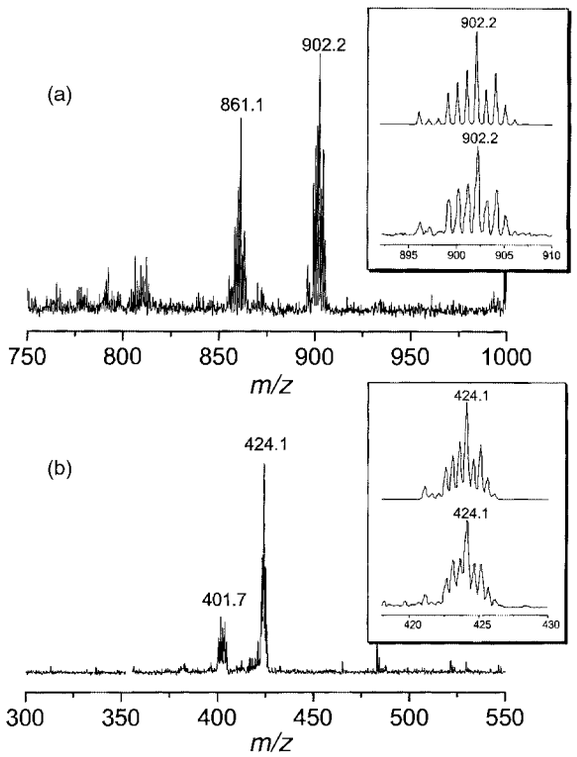

Fig. 8 Electrospray mass spectra obtained from a partly (0.7 electrons) electrolyzed ($E_{appl} = -1500$ mV) solution of L_2RuI_2 in DMF (Bu_4NPF_6). Inserts show experimental (bottom) and simulated (top) spectra of the solvated complexes (a) $[L_2RuI(DMF)]^+$ at 902.1 m/z^+ and (b) $[L_2Ru(DMF)_2]^{2+}$ centered at 424.1 m/z^+.

(b) Bulk reductive electrolysis of L_2RuI_2 in DMF and identification of products by ESMS. Further evidence for the presence of reductively induced ligand elimination described in eqn. (12)–(14) was obtained from electrospray mass spectrometric measurements. A 0.7 mM solution of L_2RuI_2 in DMF (0.01 M Bu_4NPF_6) was reductively bulk electrolyzed at a platinum gauze electrode at a potential of −1.5 V. Samples were taken during the course of the electrolysis and examined by electrospray mass spectrometry. A sample taken during an early stage (0.7 electrons per molecule transferred) is shown in Fig. 8. A series of ruthenium products is detectable in the positive ion mode. The major signal at 424.1 *m/z* is assigned to formation of the doubly charged bis-DMF complex, $[(Et_2\text{-dcbpy})_2Ru(DMF)_2]^{2+}$. The signal for the mono-DMF complex, $[(Et_2\text{-dcbpy})_2RuI(DMF)]^+$, also is detectable at 902.2 *m/z* but with less intensity. The signals at 401.7 *m/z* and 861.1 *m/z* can be assigned to complexes formed by replacement of DMF with the methanol solvent used for mass spectrometric experiments. No signals were found in the negative ion detection mode. This result is in agreement with conclusions made on the basis of cyclic voltammetric data. In another experiment, exhaustive electrolysis was carried out at −2.1V. In this case, the major ESMS peaks were found in the negative ion mode and could be assigned to the fully de-esterified bis-solvent complexes.

3.4. Electronic spectra

Absorption data obtained from electronic spectra measured in DMF are contained in Table 4b. All complexes exhibit very intense bands in the visible and UV region of the electronic spectrum. The most intense transition is found at *ca.* 31200 cm^{-1}, with molar absorbances of up to 58400 M^{-1} cm^{-1} ($L_2Ru(CN)_2$). This transition is assigned to a ligand (Et_2-dcbpy) based $\pi \longrightarrow \pi^*$ process, since the free ligand shows a transition at the same energy. Two MLCT bands, $Ru(d_\pi)Et_2$-dcbpy(π^*), of almost identical intensity, shape and absorbance are found in the visible region. The observation of two bands is a result of the energetic closeness of the π_1^* and π_2^* Et_2-dcbpy orbitals. The band at lower energies is a $d \longrightarrow \pi_1^*$ transition; the band at higher energies is the direct $d \longrightarrow \pi_2^*$ transition into the next higher unoccupied orbital.[47] The difference between the bands, ≈6300 cm^{-1} = 0.79 eV, correlates well with the spacing of the π_1^* and π_2^* orbitals of 0.6 eV obtained from MNDO calculations[16] for the free ligand. Both bands have a tail on the lower energy side, which extents to approximately 12500 cm^{-1} (L_2RuCl_2). These compounds therefore absorb almost over the whole visible region of the spectrum; this property makes this class of complexes of great importance in solar cell applications. The tail has been interpreted[42] as a spin-forbidden direct transition into the triplet state. No additional bands are observed down to 3300 cm^{-1}.

4. Conclusions

The reductive electrochemistry of L_2RuX_2 has been investigated in DMF. The presence of low lying π_1^* orbitals of the Et_2-dcbpy ligand enables up to four reversible Et_2-dcbpy ligand based one-electron reductions to be observed. The reversible potentials occur at considerably less negative potentials than reported for the bpy analogues. The degree of reversibility is associated with the stability of the reduced forms and follows the spectrochemical series. That is, reductively eliminated halides are replaced by the solvent (DMF) and the reversibility increases in the order $X = I^- < Cl^- < NCS^- < CN^-$. A competing reaction associated with decomposition of the reduced complexes is de-esterification, which gives rise to deprotonated carboxylate groups.

Spectroscopic data obtained of reduced forms of $L_2Ru(CN)_2$, such as the detection of an inter-ligand IVCT band in the NIR region of the electronic spectrum, provide evidence for the presence of spatially localized redox orbitals and electron hopping. The temperature dependence of the reversible potentials of the reduction processes also appears to be attributable to the same phenomena and can be related to the entropy imposed on the ligands by addition of one electron.

5. Acknowledgements

The authors would like to express their thanks to Dr David Humphrey for assistance in the interpretation of the electronic spectra, Dr Georgii Lazarev for recording and simulating the ESR spectra and K. L. Loening for advice on the nomenclature of Et_2-dcbpy. G. W. acknowledges a Monash Publication Award.

References

1 M. K. Nazeeruddin, A. Kay, I. Rodicio, R. Humphry-Baker, E. Muller, P. Liska, N. Vlachopoulos and M. Grätzel, *J. Am. Chem. Soc.*, 1993, **115**, 6382.
2 G. Wolfbauer, A. M. Bond, G. B. Deacon, D. R. MacFarlane and L. Spiccia, *J. Am. Chem. Soc.*, 1999, in the press.
3 A. M. Bond, G. B. Deacon, J. Howitt, D. R. MacFarlane, L. Spiccia and G. Wolfbauer, *J. Electrochem. Soc.*, 1999, **146**, 648.
4 V. Shklover, M. K. Nazeeruddin, S. M. Zakeeruddin, C. Barbe, A. Kay, T. Haibach, W. Steurer, R. Hermann, H. U. Nissen and M. Grätzel, *Chem. Mater.*, 1997, **9**, 430.
5 A. Juris, V. Balzani, F. Barigelletti, S. Campagna, P. Belser and A. Zelewsky, *Coord. Chem. Rev.*, 1988, **84**, 85.
6 M. R. McDevitt and A. W. Addison, *Inorg. Chim. Acta*, 1993, **204**, 141.
7 N. E. Tokel-Takvoryan, R. E. Hemingway and A. J. Bard, *J. Am. Chem. Soc.*, 1973, **95**, 6582.
8 G. A. Heath, L. J. Yellowlees and P. S. Braterman, *Chem. Phys. Lett.*, 1982, **92**, 646.
9 G. A. Heath, L. J. Yellowlees and P. S. Braterman, *J. Chem. Soc., Chem. Commun.*, 1981, 287.
10 D. E. Morris, K. W. Hanck and M. K. DeArmond, *J. Am. Chem. Soc.*, 1983, **105**, 3032.
11 Y. Ohsawa, M. K. DeArmond, K. W. Hanck, D. E. Morris, D. G. Whitten and P. E. Neveux Jr., *J. Am. Chem. Soc.*, 1983, **105**, 6522.

12 A. G. Motten, K. W. Hanck and M. K. DeArmond, *Chem. Phys. Lett.*, 1981, **79**, 541.
13 M. Schröder and T. A. Stephenson, in *Comprehensive Coordination Chemistry*, ed. G. Wilkinson, R. D. Gillard and J. A. McCleverty, Pergamon Press, Oxford, 1989, ch. 45, pp. 277–499.
14 R. J. Donohoe, C. D. Tait, M. K. DeArmond and D. W. Wertz, *J. Phys. Chem.*, 1986, **90**, 3927.
15 R. J. Donohoe, C. D. Tait, M. K. DeArmond and D. W. Wertz, *J. Phys. Chem.*, 1986, **90**, 3923.
16 Y. Ohsawa, M. H. Whangbo, K. W. Hanck and M. K. DeArmond, *Inorg. Chem.*, 1984, **23**, 3426.
17 Y. Sun and M. K. DeArmond, *Inorg. Chem.*, 1994, **33**, 2004.
18 D. E. Morris, K. W. Hanck and M. K. DeArmond, *J. Electroanal. Chem.*, 1983, **149**, 115.
19 D. E. Morris, K. W. Hanck and M. K. DeArmond, *Inorg. Chem.*, 1985, **24**, 977.
20 C. M. Elliott, *J. Chem. Soc.*, *Chem. Commun.*, 1980, 261.
21 C. M. Elliott and E. J. Hershenhart, *J. Am. Chem. Soc.*, 1982, **104**, 7519.
22 C. M. Elliott and J. G. Redepenning, *J. Electroanal. Chem.*, 1986, **197**, 219.
23 P. S. Braterman, G. A. Heath, A. J. MacKenzie, B. C. Noble, R. D. Peacock and L. J. Yellowlees, *Inorg. Chem.*, 1984, **23**, 3425.
24 V. T. Coombe, G. A. Heath, A. J. MacKenzie and L. J. Yellowlees, *Inorg. Chem.*, 1984, **23**, 3423.
25 G. A. Heath, in *Molecular Electrochemistry of Inorganic, Bioinorganic and Organometallic Compounds*, ed. A. J. L. Pombeiro and J. A. McCleverty, Kluwer Academic Publishers, The Netherlands, 1993, pp. 533–547.
26 E. A. V. Ebsworth, D. W. H Rankin and S. Cradocj, in *Structural Methods in Inorganic Chemistry*, Blackwell Scientific Publications, Oxford, 2nd edn., 1994, ch. 10, pp. 395–460.
27 M. Heilmann, F. Baumann, W. Kaim and J. Fiedler, *J. Chem. Soc.*, *Faraday Trans.*, 1996, **92**, 4227.
28 B. P. Sullivan, D. Conrad and T. J. Meyer, *Inorg. Chem.*, 1985, **24**, 3640.
29 P. S. Braterman, J. I. Song and R. D. Peacock, *Spectrochim. Acta*, *Par A*, 1992, **48**, 899.
30 J. L. Walsh and B. Durham, *Inorg. Chem.*, 1982, **21**, 329.
31 G. Wolfbauer, A. M. Bond and D. R. MacFarlane, *Inorg. Chem.*, 1999, **38**, 3836.
32 A. J. Fry, in *Laboratory Techniques in Electroanalytical Chemistry*, P. T. Kissinger and W. R. Heineman (eds.), Marcel Dekker Inc., New York, 2nd edn., 1996, ch. 15, pp. 469–486.
33 A. J. Bard and L. R. Faulkner, in *Electrochemical Methods*, John Wiley & Sons Inc., New York, 1980, ch. 8.3, pp. 283–298.
34 D. C. Coomber, D. J. Tucker and A. M. Bond, *J. Electroanal. Chem.*, 1997, **426**, 63.
35 D. C. Coomber, D. J. Tucker and A. M. Bond, *Analyst*, 1997, **122**, 1587.
36 R. D. Webster and A. M. Bond, *J. Org. Chem.*, 1997, **62**, 1779.
37 R. D. Webster, A. M. Bond and T. Schmidt, *J. Chem. Soc.*, *Perkin Trans. 2*, 1995, 1365.
38 H. D. Abruña, A. Y. Teng, G. J. Samuels and T. J. Meyer, *J. Am. Chem. Soc.*, 1979, **101**, 6745.
39 A. Launikonis, P. A. Lay, A. W. H. Mau, A. M. Sargeson and W. H. F. Sasse, *Aust. J. Chem.*, 1986, **39**, 1053.
40 M. K. DeArmond and C. M. Carlin, *Coord. Chem. Rev.*, 1981, **36**, 325.
41 E. König and S. Kremer, *Chem. Phys. Lett.*, 1970, **5**, 87.
42 Y. Tachibana, J. E. Moser, M. Grätzel, D. R. Klug and J. R. Durrant, *J. Phys. Chem.*, 1996, **100**, 20056.
43 T. Hannappel, B. Burfeindt, W. Storck and F. Willig, *J. Phys. Chem. B*, 1997, **101**, 6799.
44 R. J. Ellingson, J. B. Asbury, S. Ferrere, H. N. Ghosh, J. R. Sprague, T. Q. Lian and A. J. Nozik, *J. Phys. Chem. B*, 1998, **102**, 6455.
45 W. Kaim, *Coord. Chem. Rev.*, 1987, **76**, 187.
46 D. F. Shriver, P. W. Atkins and C. H. Langford, in *Inorganic Chemistry*, Oxford University Press, Oxford, 2nd edn., 1996, ch. 15, pp. 618–658.
47 M. G. Posse, N. E. Katz, L. M. Baraldo, D. D. Polonuer, C. G. Colombano and J. A. Olabe, *Inorg. Chem.*, 1995, **34**, 1830.

Paper 9/06920H